A double-layer light shutter consisting of polymer dispersed liquid crystal and azo dye/quantum dot

Oğuz Köysal[a,*], Helen F. Gleeson[b], and Gülsüm Kocakülah[a]

[a] *Department of Physics, Faculty of Arts & Sciences, Düzce University, 81620, Düzce, Turkey*

[b] *School of Physics and Astronomy, University of Leeds, Leeds, LS2 9JT, UK*

[*]Corresponding author
E-mail: oguzkoysal@gmail.com

A double-layer light shutter consisting of polymer dispersed liquid crystal and azo dye/quantum dot

Abstract

We have developed a double-layer liquid crystal light shutter and investigated its temperature dependent morphological, electro-optical, and dielectric properties. The optical layers of the shutter are in direct contact, reducing optical losses. The shutter comprises a polymer dispersed liquid crystal film adjacent to an azo dye methyl red and CdSeS/ZnS quantum dot doped cholesteric liquid crystal layer. This novel double-layer light shutter device is switchable between opaque and transparent states at room temperature, and it exhibits low threshold and saturation voltages. Both the threshold (V_{th}) and saturation (V_{sat}) voltages are found to decrease with increasing temperature. The electrical characteristics of the shutter, namely the real part of dielectric constant (ε') and the ac conductivity (σ_{ac}) also increase with temperature in the low frequency region. Our results show that this double-layer light shutter has interesting potential for simple electro-optical devices and smart window applications.

Keywords: Azo dye, cholesteric liquid crystal, light shutter, polymer dispersed liquid crystal, quantum dot.

1. Introduction

Switchable light shutters are currently attracting much attention as next-generation optical devices. In particular, light shutters produced using liquid crystals and polymers are considered to be extremely important because both liquid crystal (LC) and polymer materials are known for their low production costs, ease of preparation, and potential for mechanical and optical flexibility. Especially, polymer dispersed liquid crystal (PDLC) and cholesteric liquid crystal (CLC) structures are considered to show great potential for smart window device applications [1-5]. PDLCs, which are widely used in smart window system applications, are prepared from mixtures of low-molecular-mass nematic liquid crystal (NLC) which are dispersed in polymers, such as poly(vinyl alcohol), poly(vinyl acetate), or acrylic copolymers in the form of micro droplets [6-8]. They are usually employed in sandwich cells, i.e. the polymer/LCs droplet composites are placed between conducting glass substrates or polymer films [9]. PDLCs operate according to the scattering principle of light therefore there is no need to use polarizers in the devices, a significant advantage in terms of both light transmission and cost. An important detail in optimising the optical properties of PDLCs is matching the refractive index of the polymer matrix (n_p) and the ordinary refractive index of the LC mixture (n_o) so that the initial non-transparent (scattering) state becomes optically transparent under application of an electric field [10, 11]. CLCs are also known for their use in smart window systems. CLCs are prepared by adding chiral dopants to NLC mixtures and the resulting helical structure that characterizes these materials can act (and be considered as) as a one-dimensional photonic crystal [12, 13]. The physical properties of these materials are usually very sensitive to temperature and electric fields [14, 15]. CLCs, can exhibit planar (P), focal conic (FC), and homeotropic (H) states depending on an applied electric field, and are often preferred in light shutter device applications because of their tunability and the range of electro-optical effects that can be achieved [16-18]. In the studies carried out to date, both PDLCs and CLCs were combined with different dopant materials and the changes obtained in the mostly electro-optical parameters were emphasized. In particular, azo dye and quantum dot (QD) materials are considered important materials in improving the electro-optical properties of PDLCs and CLCs [19-23]. As is known, azo dye molecules are long and rigid, exhibiting a strong transition moment along a molecular axis, leading to anisotropic absorption of light and tending to align along the director when dissolved in the LC. Furthermore, providing high contrast ratio is the most important feature of these dyes [24]. QDs are also defined as zero-dimensional materials consisting of inorganic, metal, and

semiconductor nanoparticles with low dimensions. QDs have electro-optical and optical properties with controllable photoluminescence characteristic, core/shell geometry, tunable size. Moreover, low threshold voltage and fast response time are the most important characteristics of QDs [25, 26].

Light shutter technology is basically based on the principle of scattering and absorption of the light. PDLC and CLC composites, some of whose features are mentioned above, are among the light shutters based on light scattering. These devices can cover the background but cannot provide a colour. To realize colour surface, light shutters based on light absorption, such as a dye doped LC device, have been proposed. However, light shutters based on light absorption cannot completely block the background [27]. Thereupon, researchers have focused on device designs where both light scattering and absorption can be achieved simultaneously. There are some examples where CLC-based double-layer light shutters have been explored, usually with the aim of maximising the reflected light bandwidth or intensity. Although, in such studies, the double layers are fabricated as two separate thin film devices in separate cells and pasted on top of each other [16, 28, 29]. This approach has several drawbacks, including low light transmittance in the transparent state due to reflection losses at the multiple interfaces and high production cost due to the increase in thickness. In some cases, the added thickness can also cause parallax problems. Combining two complementary structures, such as a PDLC and CLC in a single device for applications such as smart window systems can be highly desirable. Doing so can allow novel optics to be developed while avoiding the problems associated with combining two or more separate devices mentioned above. Oh et al. produced a light shutter containing PDLC and CLC structures using a single cell and examined the light transmittance for different situations [30]. That study has been a source of motivation for us as we wished to explore in detail the electro-optical and dielectric properties of such devices.

In this paper, we describe the production of a double-layer light shutter and report its temperature-dependent morphological, electro-optical, and dielectric properties. This double-layer light shutter consists of a PDLC layer and a CLC layer containing methyl red (MR) azo dye and CdSeS/ZnS QD. Thus, the proposed double-layer light shutter can provide light absorption and scattering simultaneously with MR azo dye and LC molecules. Additionally, there is the effect of QD on the low threshold voltage of this light shutter. Moreover, examining the changes in threshold voltage, contrast ratio, and dielectric constant parameters depending on temperature is the novel aspect of the study. In conclusion, the data obtained as

a result of the evaluations show that this double-layer light shutter is promising for simple large-area see-through displays and smart windows.

2. Materials and methods

2.1. The double-layer device

A schematic of the double-layer light shutter is given in Figure 1(a and b). The first layer consists of a PDLC and the second layer, which is in direct contact with the first, consists of an azo dye MR and CdSeS/ZnS QD doped CLC composite. The light shutter allows for both opaque and transparent states. The opaque state, V=0 (Figure 1(a)), is achieved via absorption by the MR azo dye in the CLC layer and scattering by the PDLC film. The CLC mixture itself has a pitch of ~2.27 μm, so does not contribute to the visible optics through selective reflection, rather its helical structure ensures polarization-independent absorption of light by the MR. The CLC pitch is slightly longer than that chosen by Oh et al. [30] and represents ~4 rotations within the 10 μm thick CLC layer in the device. The transparent state (V≠0 (Figure 1(b)) is homeotropic and is achieved by applying a sufficiently large voltage to the device. In this state, light absorption is a minimum in the doped CLC layer and the PDLC is in the non-scattering (index-matched) configuration. Furthermore, the reason for incorporating QDs into the CLC composite is that previous studies in the literature observed that the threshold voltage values of both NLC and PDLC decreased significantly with the inclusion of QD [31-33]. Moreover, it was observed that the transition threshold voltage decreased in our previous studies with CdSeS/ZnS QD, which was preferred in this study [34, 35]. As is known, the physical properties of LCs vary depending on their molecular structure and intermolecular interactions. For example, when LCs contact a solid surface, the average orientation of the molecules is determined by the molecular structure of the LC and its interaction with the solid surface. The anchoring strength is defined as the orientation of LC molecules relative to the surface. In MR and QD doped double-layer light shutter, it is expected that the transition threshold voltage values will decrease due to the changes in the topological structure and the changing anchoring strength, especially as the molecular arrangement of the LC molecules around the QDs changes.
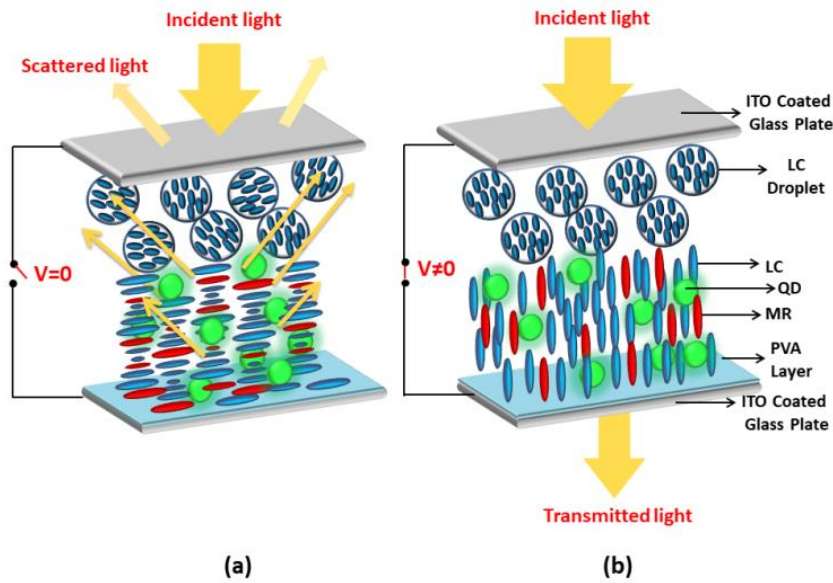
Figure 1. A schematic diagram of the double-layer light shutter. In the PDLC layer, LC droplets are suspended in a polymer matrix, while the CLC layer includes quantum dots and methyl red dye. (a) In the ground state (V=0), incident light is scattered and absorbed. (b) The high-field state (V≠0) gives approximately homeotropic alignment of the mesogens, maximising the light transmission of both layers.

2.2. Materials

In this study, E7 NLC, Norland Optical Adhesive 65 (NOA65) photopolymer, S-811 chiral dopant, azo dye MR and CdSeS/ZnS QD materials were used. The chemical structures of E7 NLC, NOA65 photopolymer, S-811 chiral dopant, MR azo dye, and schematic representation of CdSeS/ZnS QD were given in Figure 2(a-e). The properties of these materials are given below:

• The NLC mixture E7 comprises: 51% 4-pentyl-4′-cyanobiphenyl (5CB); 25% 4-heptyl-4′-cyanobiphenyl (7CB); 16% 4-octyl-4′-cyanobiphenyl (8OCB); and 8% 4-pentyl-4′-cyanoterphenyl (5CT). E7 was obtained from Instec and used both in the PDLC layer and as the host for the CLC mixture. The extraordinary and ordinary refractive indices of E7 are n_e=1.7472, n_o=1.5217, respectively at λ=589 nm [36, 37]. The nematic to isotropic phase transition temperature (T_{N-I}) is 60.5 ˚C.

• NOA65 is an ultraviolet (UV)-curable photopolymer from Norland Products with a refractive index of 1.52. NOA65 polymer comprises thiol-ene-based photomers; triallyl isocyanurate (55%), pentaerythritol tetrakis(2-mercaptopropanoate) (41%), and benzophenone

(4%) were used as photoinitiators. When cured by UV light (maximum absorption between 350-380 nm), NOA65 becomes a flexible, colourless polymer [38].

• S-811, purchased from Daken Chemical Limited, is left handed chiral dopant with a helical twisting power (*HTP*) of ~11 μm^{-1}.

• Methyl Red (MR) is a dichroic azo dye provided by Sigma-Aldrich with an absorption spectrum shown in Figure 3. The reason for preference MR as doping agent is that it has high degree of alignment capability in LC materials. Moreover, the highest possible solubility of 2 wt% MR azo dye in E7 NLC is among our reasons for preference [39-42].

• CdSeS/ZnS QDs (Linear Formula: CdS_xSe_{1-x}/ZnS), of alkyl functionalized with 6 nm diameter and emission wavelength of 525 nm, were dissolved in a toluene suspension (1 mg/mL), and organically stabilized with an oleic acid ligand coating. This material was also supplied by Sigma-Aldrich.
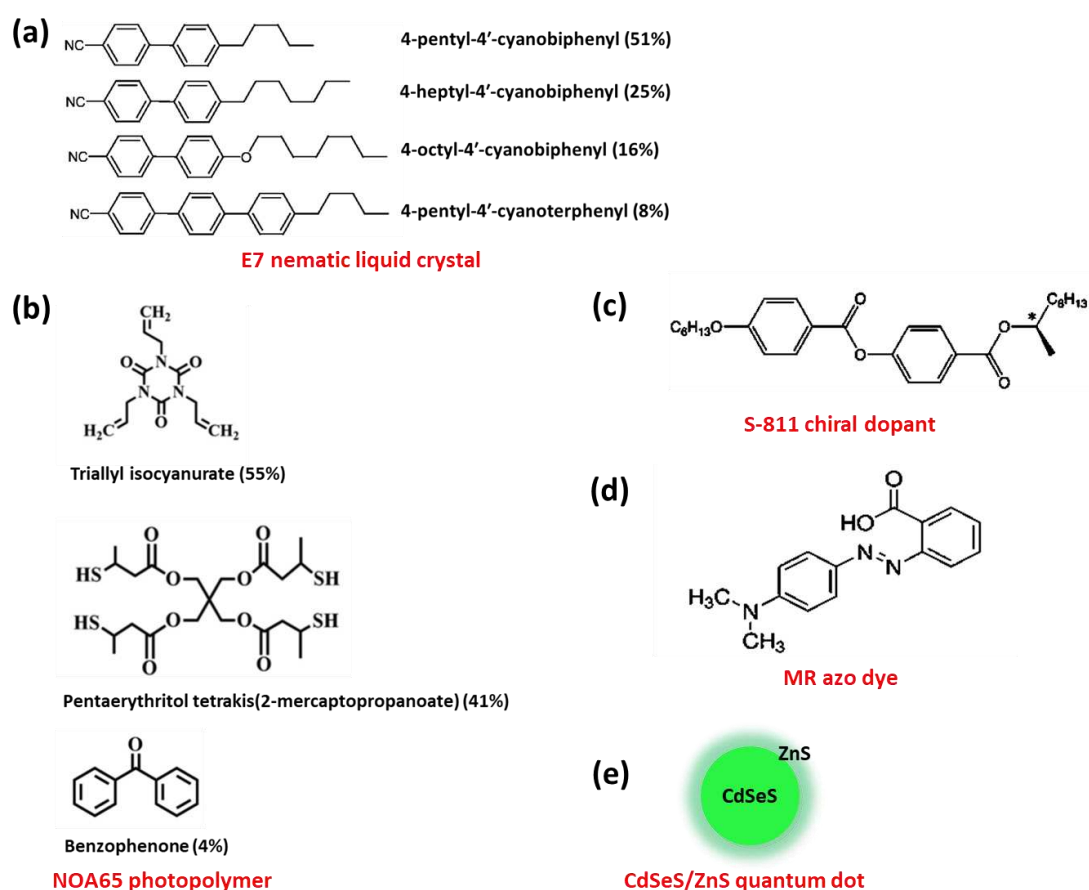
Figure 2. The chemical structures of (a) E7 NLC, (b) NOA65 photopolymer, (c) S-811 chiral dopant, (d) MR azo dye, and schematic representation of (e) CdSeS/ZnS QD.
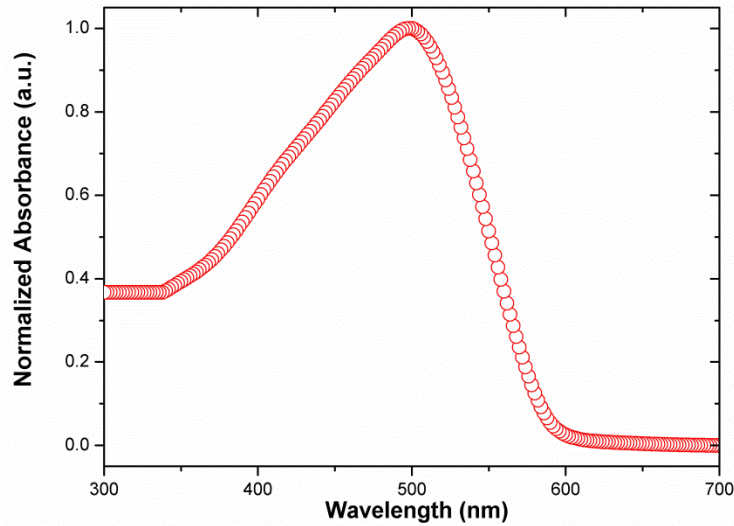
Figure 3. Normalized absorption spectrum of the MR dye.

2.3. Sample and device preparation

The sample preparation and fabrication process of the double-layer light shutter is given below:

• The PDLC layer of light shutter was prepared with NOA65 (40 wt%) and E7 (60 wt%). These proportions were chosen as they were known to give a transmittance of ~80% for the PDLC layer [30]. The NOA65/E7 mixture was incubated in an ultrasonic bath for 4 hours at 60 °C. The second layer of the double-layer light shutter, CLC, was also prepared with E7 NLC (96 wt%) and S-811 (4 wt%) chiral dopant. The prepared CLC was mixed in an ultrasonic bath for 2 hours at 60 °C and then the azo dye MR (2 wt%) and CdSeS/ZnS QD (1.5 wt%) were dispersed into the mixture. This composite was incubated in an ultrasonic bath for 6 hours at 60 °C for homogenous distribution.

• In order to prepare the PDLC structure, which is the first layer of the double-layer light shutter, an empty LC cell was used. This LC cell consists of Indium Tin Oxide (ITO) coated glass plates and 10 µm polyimide film as a spacer. The LC cell was filled with the PDLC mixture by capillary action on hot plate. The cell was then exposed to UV light of a 10 mW/cm^2 for 1 hour. After UV curing, one ITO glass substrate was removed and this structure formed the first layer of the final device. Then, PVA (Polyvinyl Alcohol) was coated onto another ITO coated glass as an alignment layer and combined with the PDLC cell using a 10 µm polyimide film as a spacer. The MR/QD doped CLC composite mixture was injected as the second layer into this cell and finally, the formation of double-layer light shutter was completed.

2.4. Measurements

The optical textures of the double-layer light shutter were examined via polarising microscopy (POM) using a DM 2700M polarised light microscope (Leica Microsystems Ltd.) equipped with a pair of linear polarisers, a Nikon D3000 camera and a Linkam T95 Peltier hot stage for temperature control. Thermo-optic behaviour, such as phase transitions and LC textures, were observed between 25 ˚C and 60 ˚C via POM. The sample was viewed under crossed polarisers with a 50x objective lens. Images were recorded under applied voltages of 0-150 V_{rms} (1 kHz square wave) to investigate the influence of electric fields on the configuration and alignment of both the LC droplets inside the polymer structure and the CLC composite layer. Cross-sectional images of the double-layer light shutter were obtained by Scanning Electron Microscopy (SEM), (FEI Quanta).

The electro-optical response of the double-layer light shutter was determined by voltage-dependent transmittance measurements. Light transmission spectra of the samples were measured under single polarisers between 400 and 700 nm, as a function of both temperature and applied voltage using a modified Olympus BH-2 microscope coupled to an HR4000 high-resolution spectrophotometer (Ocean Optics). The dielectric properties of the light shutter were determined in the frequency range 100 Hz-10 MHz with a computer-controlled Novocontrol broadband dielectric system connected to a ZG2 test interface at temperatures between 25 ˚C and the device's maximum operating temperature of 50 ˚C (below the transition to the isotropic state).

3. Results and discussion

3.1. Morphological and electro-optical measurements

We observed the cross-sectional image of the double-layer light shutter by SEM. This measurement confirmed that a high-quality double-layer structure had been formed, as well as determining the thickness of each of the layers. To undertake the SEM imaging, the double-layer device was immersed in hexane for four days to extract the LC from both the PDLC and CLC parts of the structure. Figure 4 presents the cross-sectional SEM image of the device: the top and bottom layers show ITO coated glass; the black-coloured layer is the MR/QD doped CLC layer and the dark grey layer is the PDLC structure. Figure 4 confirms that the total cell thickness is approximately ~20 μm as would be expected from the fabrication methodology if the two layers remain both intact and separate. It is also seen that thickness of the PDLC film,

which is the first layer produced, and the MR azo dye and QD doped CLC layer, are each ~10 μm thick.
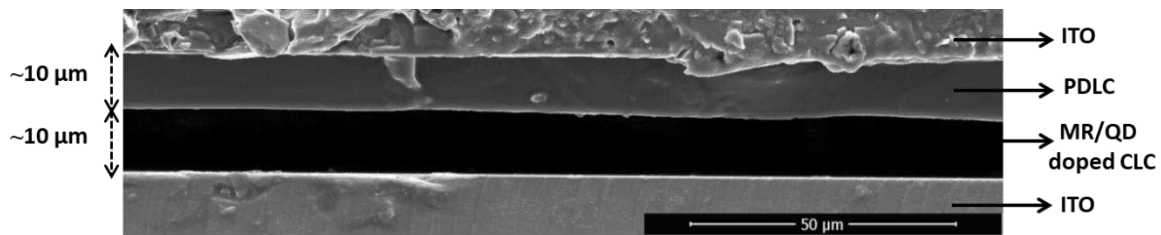
Figure 4. Cross-sectional SEM image of the double-layer light shutter.

The working temperature range of the double-layer light shutter was deduced via POM through determination of the phase transition temperatures and observation of the temperature-dependent texture changes. In Figures 5(a-f), POM images of the device are shown in the field off state. In this case, the CLC and azo dye molecules are aligned parallel to the ITO substrate and the PDLC layer is scattering. Figure 5(a) shows the completely dark isotropic state at 60 ˚C; the PDLC layer will still scatter light due to the mismatch between the polymer and isotropic E7 refractive index and the randomly oriented azo dye will still absorb light, but there is no remaining birefringence that would cause light to be transmitted by the crossed polarizers. On cooling, both the PDLC and CLC layers will transition into the isotropic phase at approximately the same temperature as each layer is based on E7. Figures 5(b and c), show the broad phase transition of the device at around 51.5 ˚C, a process that is complete by 50 ˚C. This defines the maximum working temperature of the device. As the temperature is decreased, the order parameter and birefringence of the LC both increase, the former causing the absorption of the MR molecules to increase and the latter enhancing the scattering of the PDLC layer. In the POM image obtained at 25 °C, Figure 5(f), a relatively dark image is obtained because of these combined effects. A transition temperature of 51.5 ˚C is used as a reference for the electro-optical and dielectric measurements described later.
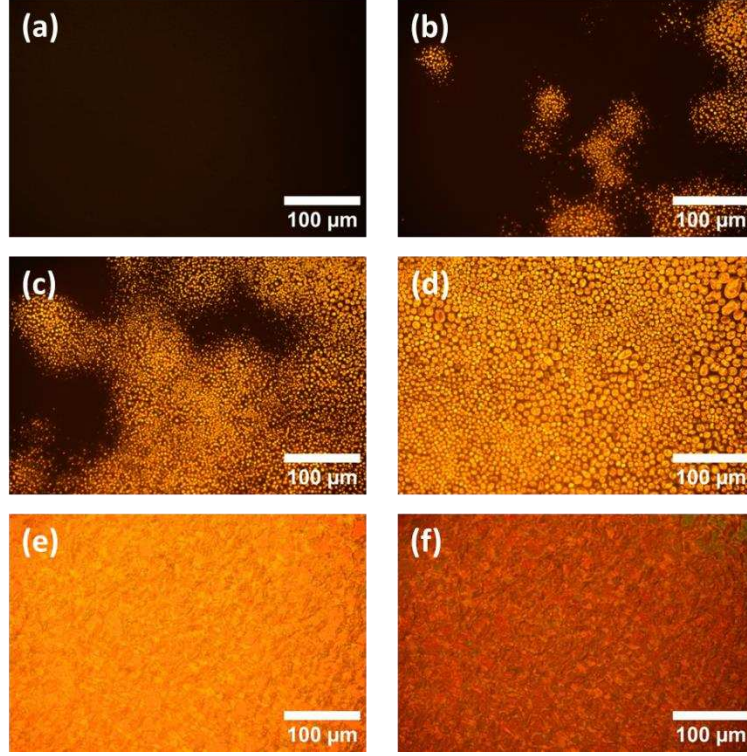
Figure 5. POM images of the double-layer light shutter viewed with crossed polarizers, field-off state, (a) 60 ˚C, (b) 52 ˚C, (c) 51.5 ˚C, (d) 50 ˚C, (e) 40 ˚C, and (f) 25 ˚C observed during the cooling process.

The temperature-dependent normalized transmitted light intensity of the double-layer light shutter measured as a function of applied voltage, is shown in Figure 6. This graph was obtained by selecting a wavelength of 632.8 nm in the transmission spectra for analysis, increasing the voltage step by step, and recording the light intensity. When the electric field is applied to the double-layer light shutter, the transmittance starts to increase sharply at a threshold voltage (V_{th}) and then starts to at saturate at a voltage (V_{sat}). The V_{th} and V_{sat} values represent the voltages required for the transmittance to reach 10% (T_{10}) and 90% (T_{90}), respectively [43, 44]. Both parameters shift to lower voltage values with increasing temperature, as seen in Figure 7.

As seen in Figure 7, the value of V_{th} decreases with increasing temperature. This is explained for both the PDLC and CLC structures through equations (1) to (3) [45-47]:

$$V_{th(PDLC)} = \frac{d}{R}\left(\frac{K(l^2-1)}{\varepsilon_o \Delta\varepsilon}\right)^{1/2} \tag{1}$$

$$V_{sat(PDLC)} = \frac{d}{R}(l^2-1)^{1/2}\frac{4\pi K}{\Delta\varepsilon} \tag{2}$$

$$V_{th(CLC)} = \frac{\pi^2 d}{p} \left(\frac{K}{\varepsilon_o \Delta \varepsilon} \right)^{1/2} \tag{3}$$

where d, K, R, l, p and $\Delta\varepsilon$ are the film thickness, an effective elastic constant (the twist elastic constant in the case of equation (3)), the droplet radius, the ratio of major to minor axes of the droplets, the helical pitch of the CLC and the dielectric anisotropy of the LC medium, respectively. From equations (1) and (3), it can be seen that $V_{th} \propto (K/\Delta\varepsilon)^{1/2}$ for both layers and that $V_{sat(PDLC)} \propto K/\Delta\varepsilon$. Mean field theory suggests that the parameters K and $\Delta\varepsilon$ change with the order parameter S according to $K \propto S^2$ and $\Delta\varepsilon \propto S$ so $V_{th} \propto S^{1/2}$ and $V_{sat(PDLC)} \propto S$. As S reduces monotonically with increasing temperature for both nematic and chiral nematic materials, V_{th} and V_{sat} values will reduce with temperature [48, 49].
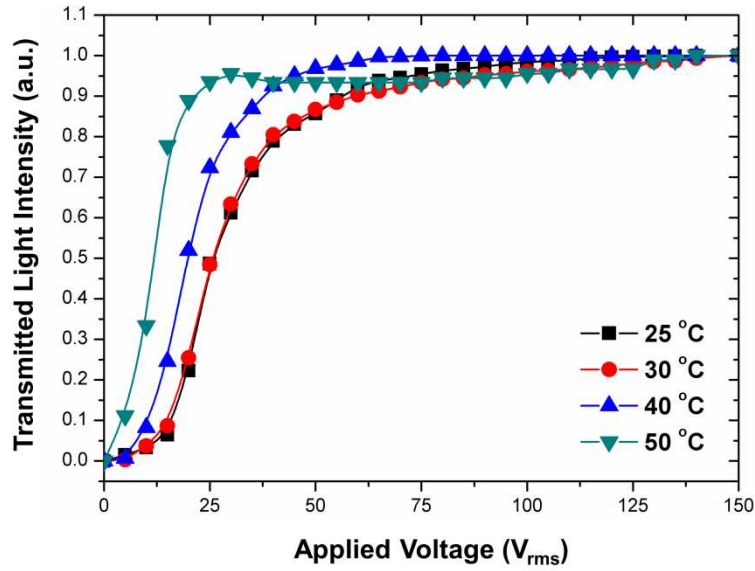
Figure 6. Transmitted Light Intensity-Applied Voltage response of the double-layer light shutter at selected temperatures.
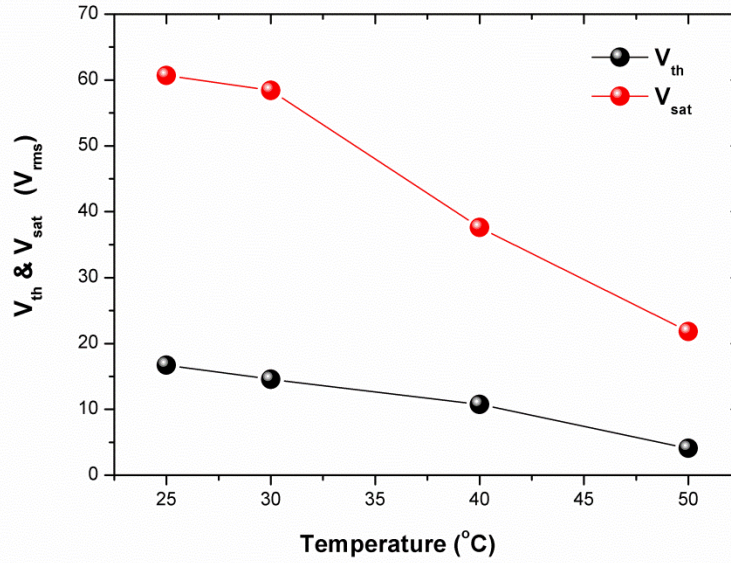
Figure 7. The behaviour of the threshold and saturation voltage values of the shutter as a function of temperature.

Figures 8(a-d) show the wavelength-dependent normalized transmitted light intensity spectra of the double-layer light shutter under single polariser with and without an applied voltage (V=150 V_{rms} and V=0 V). The spectra in the field-off state can be compared to the POM images of Figure 5(a-f). It can be seen that the transmitted light intensity in the field-off state is a minimum from 400 nm to 700 nm. The reason for this is that incident light is both scattered by the LC droplets in the PDLC layer and also absorbed by the azo dye layer. The transmitted light intensity is non-zero between 500 nm and 700 nm for V=0 V because at these wavelengths the dye is not absorbing (see Figure 3) and so only the scattering of the PDLC layer contributes to the optics of the device. At V=150 V_{rms} there is maximum transmission because both the dye molecules and the E7 in the LC droplets adopt a homeotropic orientation between 550 nm and 700 nm. However, in the presence of voltage in the wavelength range of 400-550 nm, the transmitted light intensity values of the sample are close to zero for all temperatures. This behaviour is thought to be related to the difficulty of orientation of molecules due to the high concentration of azo dye. Moreover, the absorption value of MR azo dye is high in the wavelength range of 400-550 nm and it can be interpreted that the low transmitted light intensity due to the use of high concentration dye will cause this result.
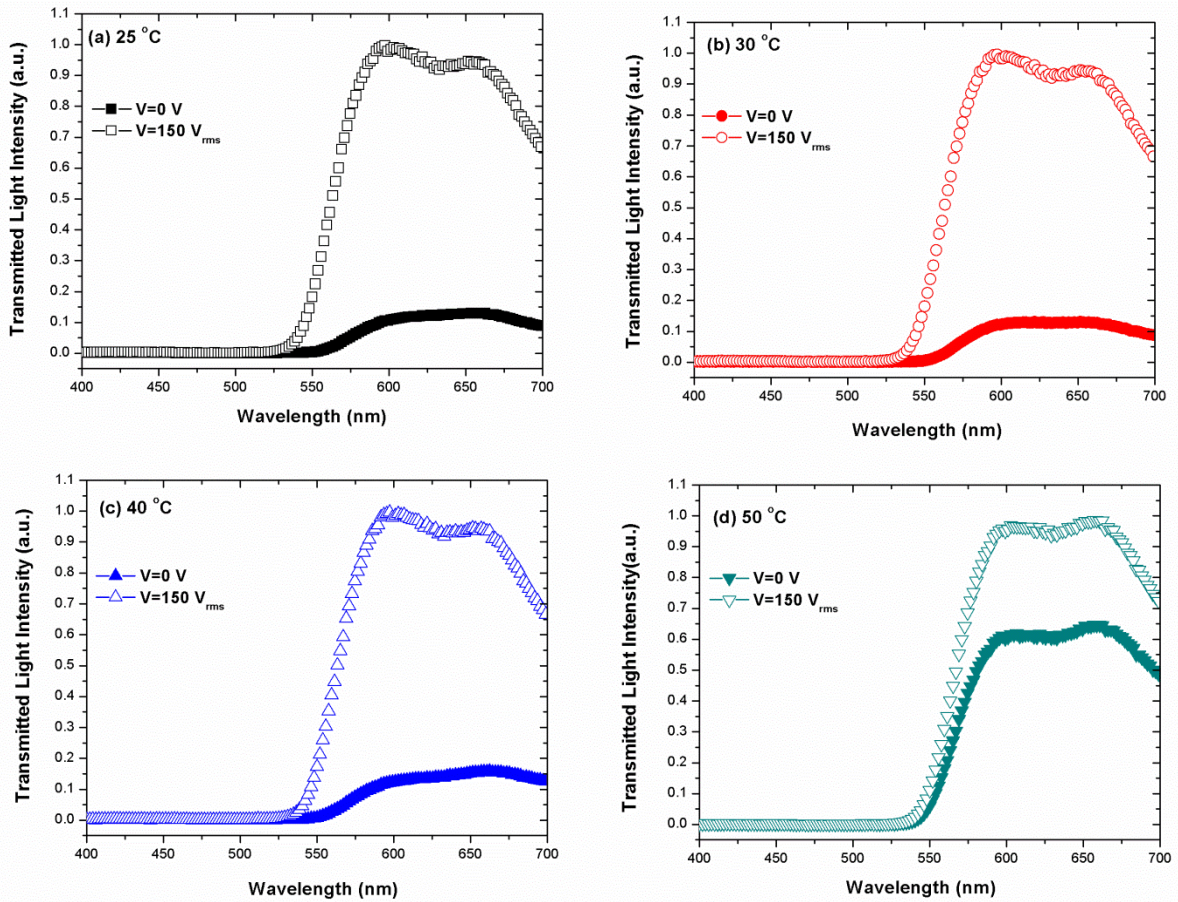
Figure 8. Transmitted Light Intensity-Wavelength graphs of the double-layer light shutter at different temperatures, (a) 25 ˚C, (b) 30 ˚C, (c) 40 ˚C, and (d) 50 ˚C.

In addition, it was observed that the temperature-dependent transmitted light intensity values of the light shutter in the voltage off state did not show a significant change from 25 °C to 40 °C. However, the transmitted light in the off reaches a maximum value at 50 °C, which is close to the phase transition temperature. This increase can be attributed to the increasingly transparent property of the sample at temperatures close to the isotropic phase; the birefringence of the E7 (and therefore scattering of the PDLC layer) reduces and the lower order parameter in the CLC layer reduces the absorption of the MR dye. In the case of voltage on, it is seen that the transmittance values of the sample take almost the same value depending on the ordered molecular orientation at all temperature values. This is because 150 V_{rms} is far higher than the saturation voltage at all temperatures.

The contrast ratio (*CR*) is obtained from the ratio of the maximum to minimum transmitted light intensity of the samples in the voltage on and voltage off states at 632.8 nm, T_{max} and T_{min} respectively, equation (4) [36, 37, 43-52]:

$$CR = \frac{T_{max}}{T_{min}} \tag{4}$$

The temperature-dependent CR of the light shutter is shown in Figure 9 where is seen that the CR slowly decreases with increasing temperature. The reason for this behaviour is that the T_{min} values increase with temperature, while the T_{max} values remain almost the same for all temperatures; the T_{min} values have a bigger influence on the variation of the CR than T_{max}. As mentioned above, the absorbance of the MR reduces with increasing temperature because the order parameter reduces, so it is the reducing order parameter that is effectively responsible for the decrease in CR.
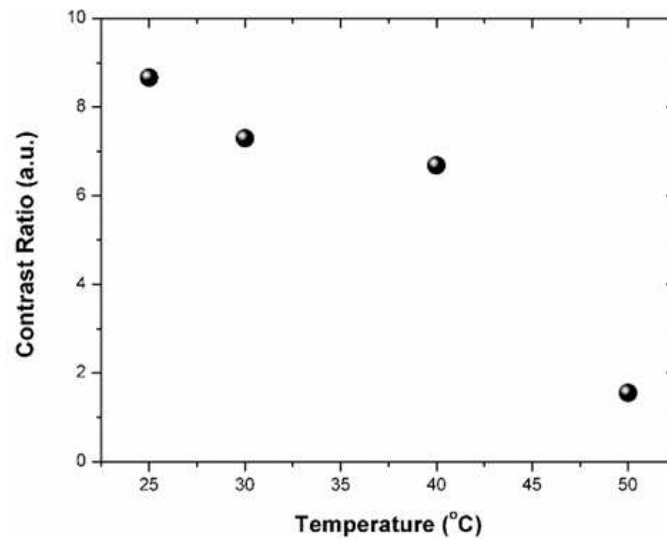
Figure 9. Temperature dependence of the contrast ratio of the double-layer light shutter.

Figures 10(a-h) show the voltage-dependent POM images of the double-layer light shutter at room temperature. It can be seen that the texture of the sample changes depending on the applied voltage, especially marked after ~30 V_{rms} and becoming almost black above ~70 V_{rms}. The POM images are compatible with the graphs in Figure 6 and Figure 8; the sample is clearly mostly homeotropic above ~70 V_{rms}.
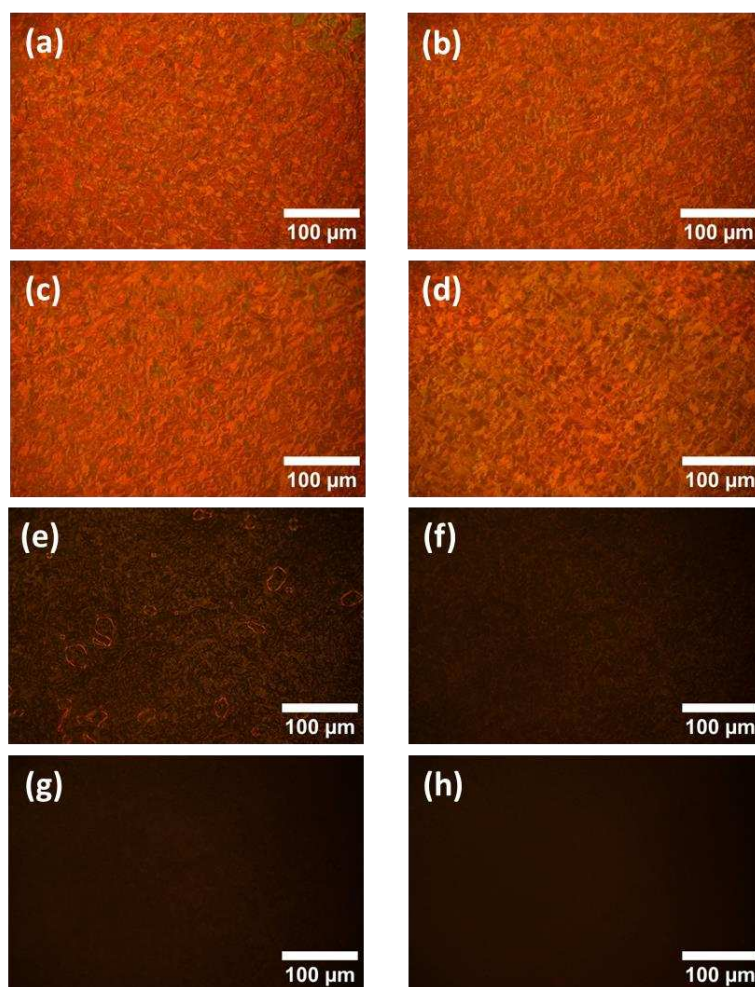
Figure 10. Voltage dependent POM images of the double-layer light shutter at room temperature at, (a) 0 V, (b) 10 V_{rms}, (c) 20 V_{rms}, (d) 30 V_{rms}, (e) 50 V_{rms}, (f) 70 V_{rms}, (g) 100 V_{rms}, and (h) 150 V_{rms}.

Photographs were also obtained to prove that the light shutter exhibits opaque and transparent properties. Figures 11(a and b) show photographs and POM images of the double-layer light shutter at room temperature, the off state (V=0) is opaque and the on state (V≠0) is transparent. As seen in Figure 11(a), the double-layer light shutter scatters and absorbs the incident light and hides the "Light Shutter" text in the background. In the transparent state (Figure 11(b)), we can clearly see the "Light Shutter" text located behind the display panel. In this state, the average refractive index of the LC droplet matches with the refractive index of the polymer structure as a result of re-orientation of the LC molecules by the electric field. Additionally, in the second layer of double-layer light shutter, the LC and MR molecules align in the direction of electric field, minimising the light absorption by the dye. The reason for the red coloured surface to be seen in Figure 11(b) is thought to be related to the difficulty in orientation of the molecules as a result of the use of high concentrations of azo dye.

16
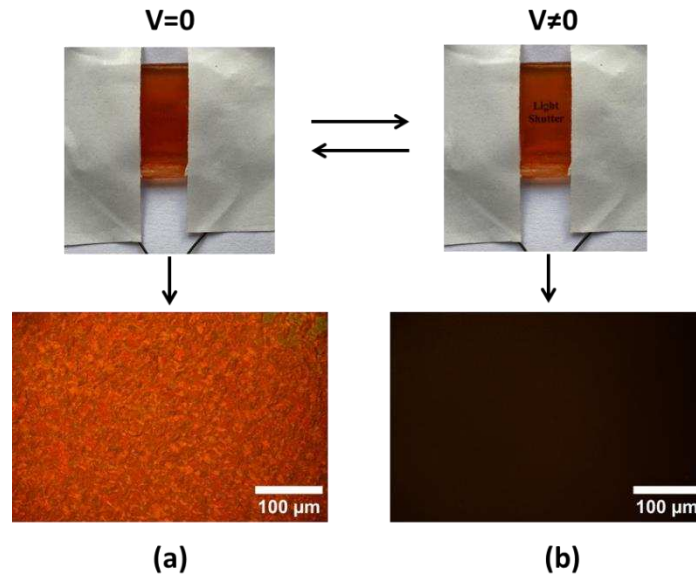
Figure 11. POM images and photographs of the double-layer light shutter at room temperature, (a) the off state (V=0) (opaque) and (b) the on state (V≠0) (transparent).

Finally, in terms of the optics, it is appropriate to consider whether the double-layer light shutter operates more advantageously than a single-layer device. Figure 12 gives a comparison between the transmittance of a single-layer PDLC structure and this double-layer structure. It can be seen that the addition of the MR/QD doped CLC layer significantly improves the opacity of the device at all wavelengths, but especially in the 400-550 nm regime where the absorbance of the MR is highest. Clearly, this light shutter offers much improved optical properties in comparison to a single-layer PDLC.
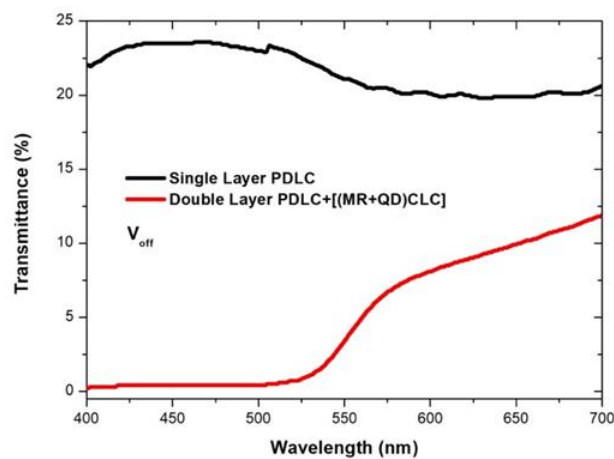
Figure 12. A comparison of the transmittance of a single-layer PDLC device and this double-layer PDLC and doped CLC device in the field-off state.

3.2. Dielectric measurements

Dielectric properties have a very important role in determining the characteristics and basic parameters of PDLC devices. Furthermore, studying the dielectric behaviour of liquid crystals offers a tool to give insight into molecular relaxation behaviour which changes significantly as a function of temperature as well as with liquid crystal structure and the inclusion of dopants. There are many studies of the electrical properties of doped CLC devices and PDLC devices, reflecting their general use as separate entities in almost all applications [24, 53-56]. We have used dielectric studies to gain insight into the electrical response of the double-layer structure, with intimately integrated CLC and PDLC layers, as a function of frequency. In this case, the inclusion of the quantum dots in the composite CLC layer is expected to provide additional features to the electrical response.

The dielectric properties a material can be expressed as follows [57, 58]:

$$\varepsilon^* = \varepsilon' - i\varepsilon'', \tag{5}$$

where ε' and ε'' are the real and imaginary parts of the complex dielectric constant ε^*, related to electrical storage and loss in the material respectively. The ε' and ε'' graphs depending on the frequency of the double-layer light shutter are given in Figure 13(a and b). Additionally, frequency dependent ε' and ε'' graphs for single-layer PDLC are also seen as inset in Figure 13(a and b). The behaviours of ε' as a function of frequency for the double-layer light shutter at different temperatures shown in Figure 13(a), upper graph. The temperature range studied was from 25 ˚C to 50 ˚C and it can be seen that ε' has the highest value in low frequency regime (100 Hz-1 kHz) at 50 ˚C. The increase in ε' in the low frequency regime can be explained by an increase in space-charge polarization. However, it can also be seen that the value of ε' decreases with increasing frequency. This reduction is due to reduced space-charge polarization. Polarization occurs due to electron-hopping between ions in different valence states in the composite. As the frequency is increased, the electrons cannot follow the changing alternating field. These changes cause a net charge displacement and thus a decrease in the dielectric constant [24, 59, 60]. It is also seen that ε' value increases with temperature in the low frequency region. This change is thought to be related to ionic and electronic polarization and crystal defects at low temperature values. In addition, it can be interpreted that the effects occurring at high temperature values are related to thermally agitated charge carriers and impurity dipoles [61].

The temperature dependence of the dielectric loss ε'' is also shown in Figure 13(b), lower graph. In the low frequency region, it is seen that the ε'' value is high and decreases with increasing frequency. With the increase in frequency, the polarization lags behind the changing ac field, which causes a decrease in the ε'' value. It is also seen from the graph that the ε'' value increases with increasing temperature in the low frequency region and reaches its maximum value at 50 °C. However, ε'' remains almost constant with increasing temperature at high frequency values especially above 10 kHz. In addition, no relaxation peak was observed in the high frequency region of the ε''-f graph, suggesting that the sample will show relaxation behaviour in a higher frequency regime (more than 10 MHz).
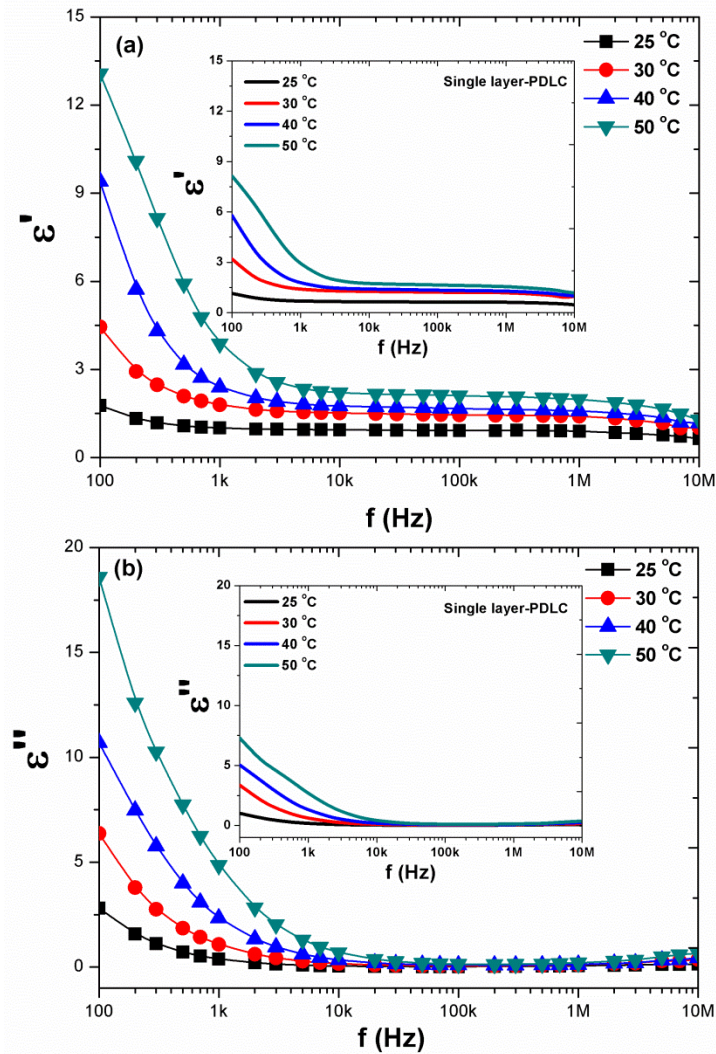
Figure 13. Temperature-dependent plots showing (a) ε' and (b) ε'' as a function of frequency measured in of double-layer light shutter (insets: ε' and ε'' graphs of single layer PDLC as a function of frequency).

We also examined the frequency dependent variation of the ac conductivity value. The ac conductivity is calculated using the following equation [62, 63]:

$$\sigma_{ac} = \varepsilon_o \omega \varepsilon'' \tag{6}$$

where ω is the angular frequency. The conductivity is shown as a function of frequency at selected temperatures in Figure 14. It is known that the conductivity value in the composite materials is formed by the hopping, mobility and transportation mechanisms of the ionic charge carriers of the samples. A frequency-independent conductivity is observed in the low frequency regime due to random diffusion of ionic charge carriers via activated hoping. On the other hand, it is observed that σ_{ac} increases with increasing frequency at all temperatures. It is also seen that at the frequency value of 10 MHz, σ_{ac} converges for all temperatures.
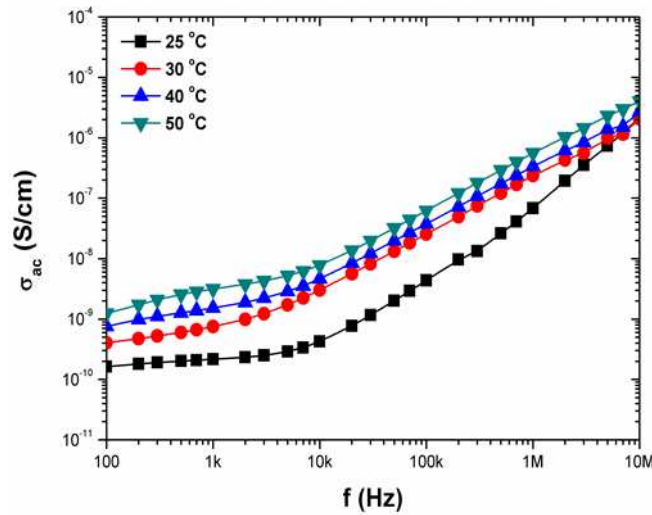
Figure 14. The conductivity of the double-layer light shutter as a function of frequency at selected temperatures.

There are limited studies in the literature examining the dielectric properties of single layer PDLC composites [24, 55, 56, 64, 65]. In addition, the number of studies examining the temperature-dependent dielectric properties of PDLCs is also very few [24, 56]. It was observed that both ε' and ε'' values of the double layer-light shutter produced in this study increased considerably when compared to the single layer PDLCs (inset graphs in Figure 13(a and b)). On the other hand, while investigating the temperature-dependent σ_{ac} values of NLCs, the number of studies investigating the σ_{ac} values of PDLCs is negligible. It is thought that the σ_{ac} values obtained within the scope of this study will be an example for other studies to be conducted. In this respect, the dielectric measurements made for the double-layer light shutter are considered to be very important.

4. Conclusion

In this study, we have investigated the temperature dependent textures, electro-optical, and dielectric properties of a new-concept double-layer liquid crystal light shutter. The maximum operating temperature range was shown to be 50 °C, effectively coinciding with the liquid crystal to isotropic phase transition temperature of each of the layers. The electro-optical data showed that both of the relevant operating voltages, V_{th} and V_{sat} decrease with increasing temperature up to 50 °C. Specifically, it was observed that the V_{th} and V_{sat} values measured at 50 °C decreased by 74% and 64%, respectively, compared to the values measured at 25 °C. A similar effect was seen for the CR, which also decreases as the temperature increases, reaching its lowest value at 50 °C. It was observed that the CR of the light shutter at 50 °C decreased by 82% compared to the CR value obtained at 25 °C. The temperature-dependent dielectric measurements show that ε' has the highest value in the low frequency region and that it reaches its maximum value at 50 °C. Similarly, ε'' value is high in the low frequency region and starts to decrease with increasing frequency. Moreover, the σ_{ac}-f graph of sample shows that σ_{ac} increase with increasing frequency at all temperatures. The results show that the both the electro-optical and dielectric properties of the double-layer light shutter change significantly depending on the temperature. Finally, we note that one of the key differences between our double-layer device and that of Oh et al. [30] is that we have used a dye that absorbs only over part of the visible spectrum, meaning that we have very different physical effects in different wavelength regimes. The use of selectively absorbing dyes offers an opportunity to tune the optics of this light shutter either for esoteric or practical reasons, showing an additional advantage of the device. Moreover, it is thought that the produced double-layer light shutter is important in terms of containing both azo dye and QD effects, together with a comprehensive investigation of the temperature-dependent electro-optical and dielectric properties. We conclude that the device has several features that could be beneficial to smart windows or simple displays. It is also thought that it may be possible to produce double-layer light shutters that can operate at higher temperatures by using liquid crystal materials with higher phase transition temperatures. Moreover, considering the results of the study, it can be concluded that double-layer light shutters of larger dimensions can be produced if suitable materials are provided. It is thought that these suggestions will provide insight to researchers in smart windows technology.

References

[1] L. Jinqian, Y. Zhao, H. Gao, D. Wang, Z. Miao, H. Cao, Z. Yang, W. He, Polymer dispersed liquid crystals doped with CeO_2 nanoparticles for the smart window, Liquid Crystals 49(1) (2022) 29-38.

[2] Z.-Y. Liang, C.-Y. Tu, T.-H. Yang, C.-K. Liu, K.-T. Cheng, Low-threshold-voltage and electrically switchable polarization-selective scattering mode liquid crystal light shutters, Polymers 10 (2018) 1354.

[3] R. Gahrotra, V. Sharma, A.R. Dogra, P. Malik, P. Kumar, Performance augmentation of bistable cholesteric liquid crystal light shutter- effect of dichroic dye on morphological and electro-optical characteristics, Optical Materials 127 (2022) 112243.

[4] X. Du, Y. Li, Y. Liu, F. Wang, D. Luo, Electrically switchable bistable dual frequency liquid crystal light shutter with hyper-reflection in near infrared, Liquid Crystals 46(11) (2019) 1727-1733.

[5] Y. Choi, S.-W. Oh, T.-H. Choi, B.-H. Yu, T.-H. Yoon, Formation of polymer structure by thermally-induced phase separation for a dye-doped liquid crystal light shutter, Dyes and Pigments 163 (2019) 749-753.

[6] D. Jayoti, P. Malik, A. Singh, Analysis of morphological behaviour and electro-optical properties of silica nanoparticles doped polymer dispersed liquid crystal composites, Journal of Molecular Liquids 225 (2017) 456-461.

[7] R.R. Deshmukh, A.K. Jain, The complete morphological, electro-optical and dielectric study of dichroic dye-doped polymer-dispersed liquid crystal, Liquid Crystals 41(7) (2014) 960-975.

[8] Y.-H. Fan, Y.-H. Lin, H. Ren, S. Gauza, S.-T. Wu, Fast-response and scattering-free polymer network liquid crystals for infrared light modulators, Applied Physics Letters 84(8) (2004) 1233-1235.

[9] V. Shibaev, Liquid Crystalline Polymers, Reference Module in Materials Science and Materials Engineering, Elsevier Inc. 2016.

[10] S.-H. Lee, T.-K. Lim, S.-T. Shin, K.-S. Park, A method for improving contrast ratio of polymer dispersed liquid crystal film using the oriented azo-dye molecules in polymer matrix, Japanese Journal of Applied Physics 41 (2002) 208.

[11] Y. Kim, K. Kim, K.B. Kim, J.-Y. Park, N. Lee, Y. Seo, Flexible polymer dispersed liquid crystal film with graphene transparent electrodes, Current Applied Physics 16 (2016) 409-414.

[12] R.S. Pathinti, B. Gollapelli, S.K. Jakka, J. Vallamkondu, Green synthesized TiO_2 nanoparticles dispersed cholesteric liquid crystal systems for enhanced optical and dielectric properties, Journal of Molecular Liquids 336 (2021) 116877.

[13] D.J. Mulder, A.P.H.J. Schenning, C.W.M. Bastiaansen, Chiral-nematic liquid crystals as one dimensional photonic materials in optical sensors, Journal of Materials Chemistry C 2 (2014) 6695-6705.

[14] Y.-S. Zhang, C.-L. Ma, V.Y. Rudyak, S.-A. Jiang, S.A. Shvetsov, J.-D. Lin, C.-R. Lin, Thermal and optical manipulation of morphology in cholesteric liquid crystal microdroplets constrained on microfibers, Journal of Molecular Liquids 328 (2021) 115383.

[15] P. Gan, X. Zhang, L. Zhao, W. Shi, H. Cao, H. Wang, Z. Yang, D. Wang, W. He, Broadband reflection in polymer-stabilized cholesteric liquid crystal film with zinc oxide nanoparticles film thermal diffusion method, Liquid Crystals 48(14) (2021) 1959-1968.

[16] J.-W. Huh, B.-H. Yu, J. Heo, T.-H. Yoon, Double-layered light shutter using long-pitch cholesteric liquid crystal cells, Applied Optics 54(12) (2015) 3792-3795.

[17] C.S. Lee, T.A. Kumar, J.H. Kim, J.H. Lee, J.S. Gwag, G.-D. Lee, S.H. Lee, An electrically switchable visible to infra-red dual frequency cholesteric liquid crystal light shutter, Journal of Materials Chemistry C 6 (2018) 4243-4249.

[18] B.-H. Yu, J.-W. Huh, J. Heo, T.-H. Yoon, Simultaneous control of haze and transmittance using a dye-doped cholesteric liquid crystal cell, Liquid Crystals 42(10) (2015) 1460-1464.

[19] P. Kumar, V. Sharma, K.K. Raina, Studies on inter-dependency of electrooptic characteristics of orange azo and blue anthraquinone dichroic dye doped polymer dispersed liquid crystals, Journal of Molecular Liquids 251 (2018) 407-416.

[20] V. Sharma, P. Kumar, A. Sharma, Chinky, K.K. Raina, Droplet configuration control with orange azo dichroic dye in polymer dispersed liquid crystal for advanced electro-optic characteristics, Journal of Molecular Liquids 233 (2017) 122-130.

[21] G. Chauhan, P. Malik, P. Malik, A. Deep, Improved performance of cadmium selenide quantum dots-doped polymer stabilized cholesteric liquid crystals for light shutter, Liquid Crystals 50(15) (2023) 2540-2551.

[22] M. Cao, S. Yang, Y. Zhang, X. Song, Y. Che, H. Zhang, Y. Yu, G. Ding, G. Zhang, and J. Yao, Tunable amplified spontaneous emission in graphene quantum dots doped cholesteric liquid crystals, Nanotechnology 28 (2017) 245202.

[23] S.-W. Oh, J.-M. Baek, S.-H. Kim, T.-H. Yoon, Optical and electrical switching of cholesteric liquid crystals containing azo dye, RSC Advances 7 (2017) 19497-19501.

[24] A. Katariya-Jain, R.R. Deshmukh, Effects of dye doping on electro-optical, thermo-electro-optical and dielectric properties of polymer dispersed liquid crystal films, Journal of Physics and Chemistry of Solids 160 (2022) 110363.

[25] G. Singh, M.R. Fisch, S. Kumar, Tunable polarised fluorescence of quantum dot doped nematic liquid crystals, Liquid Crystals 44(3) 2017 444-452.

[26] J. Mirzaei, M. Reznikov, T. Hegmann, Quantum dots as liquid crystal dopants, Journal of Materials Chemistry 22 (2012) 22350-22365.

[27] J.-W. Huh, B.-H. Yu, D.-M. Shin, T.-H. Yoon, Double-layered liquid crystal light shutter for control of absorption and scattering of the light incident to a transparent display device, Proceedings of SPIE 9384 (2015) 938417.

[28] X. Xie, P. Huang, M. Xu, Y. Ding, L. Qiu, H. Lu, Tri-state switching of a high-order parameter, double-layered guest-host liquid-crystal shutter, doped with the mesogenic molecule 4HPB, Liquid Crystals 48(11) (2021) 1555-1561.

[29] L. Komitov, G. Hegde, D. Kolev, Fast liquid crystal light shutter, Journal of Physics D: Applied Physics 44 (2011) 442002.

[30] S.-W. Oh, J.-M. Baek, J. Heo, T.-H. Yoon, Dye-doped cholesteric liquid crystal light shutter with a polymer-dispersed liquid crystal film, Dyes and Pigments 134 (2016) 36-40.

[31] X. Liu, X. Xia, L. Yang, J. Zhu, M. Xu, G. Zhang, G. Xia, L. Qui, H. Lu, Physical properties of liquid crystals doped with $CsPbBr_3$ quantum dots, Liquid Crystals 48(10) (2021) 1357-1364.

[32] A. Rastogi, K. Agrahari, G. Pathak, A. Srivastava, J. Herman, R. Manohar, Study of an interesting physical mechanism of memory effect in nematic liquid crystal dispersed with quantum dots, Liquid Crystals 46(5) (2019) 725-735.

[33] C.-C. Hsu, Y.-X. Chen H.-W., Li, J.-S. Hsu, Low switching voltage ZnO quantum dots doped polymer-dispersed liquid crystal film, Optics Express 24(7) (2016) 7063-7068.

[34] G. Kocakülah, G. Algül, Oğuz Köysal, Effect of CdSeS/ZnS quantum dot concentration on the electro-optical and dielectric properties of polymer stabilized liquid crystal, Journal of Molecular Liquids 299 (2020) 112182.

[35] G. Kocakülah, Oğuz Köysal, Electro-optical and dielectric response of quantum dot doped cholesteric liquid crystal composites, Journal of Materials Science: Materials in Electronics 33 (2022) 5489-5500.

[36] J. Li, S.T. Wu, S. Brugioni, R. Meucci, S. Faetti, Infrared refractive indices of liquid crystals, Journal of Applied Physics 97 (2005) 073501.

[37] J. Li, G. Baird, Y.-H. Lin, H. Ren, S.-T. Wu, Refractive-index matching between liquid crystals and photopolymers, Journal of the SID 13(12) (2005) 1017-1026.

[38] A. Chaudhary, R.K. Shukla, P. Rani, A. Choudhary, P. Malik, R. Mehra, K.K. Raina, Polymer dispersed liquid crystals devices: role of photopolymerisation to control defect orientation, optical and electro-optical properties, Liquid Crystals 50(6) (2023) 977-988.

[39] G. Gilardi, R. Asquini, A. d'Alessandro, R. Beccherelli, L. De Sio, C. Umeton, All optical and thermal tuning of a bragg grating based on photosensitive composite structures containing liquid crystals, Molecular Crystals and Liquid Crystals 558 (2012) 64-71.

[40] L. De Sio, J.G. Cuennet, A.E. Vasdekis, D. Psaltis, All-optical switching in an optofluidic polydimethylsiloxane: Liquid crystal grating defined by cast-molding, Applied Physics Letters 96 (2010) 131112.

[41] G. Gilardi, L. De Sio, R. Beccherelli, R. Asquini, A. d'Alessandro, C. Umeton, Observation of tunable optical filtering in photosensitive composite structures containing liquid crystals, Optics Letters 36(24) (2011) 4755-4757.

[42] L. De Sio, A.E. Vasdekis, J.G. Cuennet, A. De Luca, A. Pane, D. Psaltis, Silicon oxide deposition for enhanced optical switching in polydimethylsiloxane-liquid crystal hybrids, Optics Express 19(23) (2011) 23532-23537.

[43] H. Zhang, F. Li, K. Li, Y. Zhang, Y. Peng, Y. Lu, J. Liu, K. Diao, Y. Zhao, Z. Miao, The effect of the LC mixtures with the different clearing point on temperature dependence of the electro-optical properties of polymer dispersed liquid crystals, Molecular Crystals and Liquid Crystals 726(1) (2021) 27-40.

[44] X. Meng, J. Li, Y. Lin, X. Liu, G. Li, J. Zhao, Y. Miao, W. Li, W. Ye, D. Li, Z. He, Electro-optical response of polymer-dispersed liquid crystals doped with γ-Fe_2O_3 nanoparticles, Liquid Crystals 49(6) (2022) 855-863.

[45] H. Lin, S. Zhang, M.H. Saeed, L. Zhou, H. Gao, J. Huang, L. Zhang, H. Yang, J. Xiao, Y. Gao, Effects of the methacrylate monomers with different end groups on the morphologies, electro-optical and mechanical properties of polymer dispersed liquid crystals composite films, Liquid Crystals 48(5) (2020) 722-734.

[46] D.K. Yang, Fundamentals of liquid crystal devices, John Wiley & Sons 2014.

[47] P.G. de Gennes, Calcul de la distorsion d'une structure cholesterique par un champ magnetique, Solid State Communications 6(3) (1968) 163-165.

[48] J.-W. Han, Temperature dependence of electro-optical characteristics of polymer dispersed liquid crystal films, Liquid Crystals 28(10) (2001) 1487-1493.

[49] M.M. Mhatre, A. Katariya-Jain, R.R. Deshmukh, Enhancing morphological, electro-optical and dielectric properties of polymer-dispersed liquid crystal by doping of disperse Orange 25 dye in LC E7, Liquid Crystals 49(6) (2022) 790-803.

[50] T.-J. Chen, Y.-F. Chen, C.-H. Sun, J.-J. Wu, Electro-optical properties of reverse mode polymer dispersed liquid crystal films, Japanese Journal of Applied Physics 43(4B) (2004) L557.

[51] V. Sharma, P. Kumar, Chinky, P. Malik, K.K. Raina, Morphological and Electro Optic studies of Polymer Dispersed Liquid Crystal in Reverse Mode, AIP Conference Proceedings 1953 (2017) 100033.

[52] Y.-C. Hsiao, K.-C. Huang, W. Lee, Photo-switchable chiral liquid crystal with optical tristability enabled by a photoresponsive azo-chiral dopant, Optics Express 25(3) (2017) 2687-2693.

[53] R.S. Pathinti, B. Gollapelli, S.K. Jakka, J. Vallamkondu, Green synthesized TiO$_2$ nanoparticles dispersed cholesteric liquid crystal systems for enhanced optical and dielectric properties, Journal of Molecular Liquids 336 (2021) 116877.

[54] O. Köysal, Conductivity and dielectric properties of cholesteric liquid crystal doped with single wall carbon nanotube, Synthetic Metals 160(9-10) (2010) 1097-1100.

[55] A. Katariya-Jain, R.R. Deshmukh, Electro-optical and dielectric study of multi-walled carbon nanotube doped polymer dispersed liquid crystal films, Liquid Crystals 46(8) (2019) 1191-1202.

[56] S.S. Parab, M.K. Malik, P.G. Bhatia, R.R. Deshmukh, Investigation of liquid crystal dispersion and dielectric relaxation behavior in polymer dispersed liquid crystal composite films, Journal of Molecular Liquids 199 (2014) 287-293.

[57] M. Yıldırım, A. Allı, G. Önsal, N. Gök, O. Köysal, Synthesis & chemical and dielectric characterization of poly (linoleic acid)-g-poly (dimethylaminoethyl methacrylate): A novel high-κ graft copolymer, Composites Part B 117 (2017) 43-48.

[58] E. Orhan, M. Gökçen, O. Köysal, Performance analysis and negative dielectric anisotropy behavior of nematic liquid crystal doped with newly synthesized 1-(p-chlorobenzyl)-5-nitrobenzimidazole cobalt complex, Synthetic Metals 240 (2018) 8-14.

[59] R. Nasri, T. Missaoui, A. Hbibi, T. Soltani, Enhanced dielectric properties of nematic liquid crystal doped with ferroelectric nanoparticles, Liquid Crystals 48(10) (2021) 1429-1437.

[60] A. Rani, S. Chakraborty, A. Sinha, Effect of CdSe/ZnS quantum dots doping on the ion transport behavior in nematic liquid crystal, Journal of Molecular Liquids 342 (2021) 117327.

[61] A. Rastogi, F.P. Pandey, A.S. Parmar, S. Singh, G. Hegde, R. Manohar, Effect of carbonaceous oil palm leaf quantum dot dispersion in nematic liquid crystal on zeta potential, optical texture and dielectric properties, Journal of Nanostructure in Chemistry 11 (2021) 527-548.

[62] P. Malik, A. Chaudhary, R. Mehra, K.K. Raina, Electrooptic and Dielectric Studies in Cadmium Sulphide Nanorods/Ferroelectric Liquid Crystal Mixtures, Advances in Condensed Matter Physics 2012 (2012) 1-8.

[63] Z. Güven Özdemir, N. Yilmaz Canli, M. Kılıç, O. Köysal, Ö. Yilmaz, M. Okutan, Molecular orientation of nickel phthalocyanine doped nematic liquid crystal composite under magnetic field, Molecular Crystals and Liquid Crystals 634(1) (2016) 1-11.

[64] S. Mani, S. Patwardhan, S. Hadkar, K. Mishra, P. Sarawade, Enhanced optical and dielectric properties of polymer dispersed liquid crystal for display applications, Materials Today: Proceedings 80(2) (2022) 747-752.

[65] Z. Jiang, J. Zheng, Y. Liu, Q. Zhu, Investigation of dielectric properties in polymer dispersed liquid crystal films doped with CuO nanorods, Journal of Molecular Liquids 295 (2019) 111667.